

Supplement of Atmos. Chem. Phys., 18, 3641–3657, 2018
<https://doi.org/10.5194/acp-18-3641-2018-supplement>
© Author(s) 2018. This work is distributed under
the Creative Commons Attribution 4.0 License.



Supplement of

Modeling reactive ammonia uptake by secondary organic aerosol in CMAQ: application to the continental US

Shupeng Zhu et al.

Correspondence to: Donald Dabdub (ddabdub@uci.edu)

The copyright of individual parts of the supplement might differ from the CC BY 4.0 License.

1 Additional tables

Table S1. Definitions of the statistical parameters used in this work. o_i and c_i are the observed and the simulated concentrations at time and location i , respectively. n is the number of data. \bar{o} and \bar{c} are averaged observed and the simulated concentrations, respectively.

Statistic indicator	Definition
Root mean square error (RMSE)	$\sqrt{\frac{1}{n} \sum_{i=1}^n (c_i - o_i)^2}$
Correlation	$\frac{\sum_{i=1}^n (c_i - \bar{c})(o_i - \bar{o})}{\sqrt{\sum_{i=1}^n (c_i - \bar{c})^2} \sqrt{\sum_{i=1}^n (o_i - \bar{o})^2}}$
Mean normalised gross bias (MNGB)	$\frac{1}{n} \sum_{i=1}^n \frac{o_i - c_i}{c_i}$
Mean normalised gross error (MNGE)	$\frac{1}{n} \sum_{i=1}^n \frac{ o_i - c_i }{c_i}$
Mean fractional bias (MFB)	$\frac{1}{n} \sum_{i=1}^n \frac{c_i - o_i}{(c_i + o_i)/2}$
Mean fractional error (MFE)	$\frac{1}{n} \sum_{i=1}^n \frac{ c_i - o_i }{(c_i + o_i)/2}$

Table S2. Comparison between simulation results for PM₁₀ and observations from the AQS network. (Obs. stands for observation; Sim. stands for simulation. Corr. stands for correlation; No. Sites means number of observation site used for statistics.)

Scenario	Period	Obs. mean	Sim. mean	RMSE	Corr.	MFB	MFE	No. Sites
		$\mu\text{g}/\text{m}^{-3}$	$\mu\text{g}/\text{m}^{-3}$	$\mu\text{g}/\text{m}^{-3}$	%	%	%	
Base	Summer	26.6	28.6	34.5	7.8	14.1	63.0	225
$\gamma=10^{-3}$	Summer	26.6	30.4	36.1	7.8	17.8	65.0	225
$\gamma=10^{-4}$	Summer	26.6	28.7	34.7	7.8	14.6	63.3	225
$\gamma=10^{-5}$	Summer	26.6	28.6	34.5	7.8	14.2	63.0	225
Base	Winter	19.7	16.0	24.3	13.8	-8.8	65.9	229
$\gamma=10^{-3}$	Winter	19.7	15.6	24.2	13.9	-10.4	65.6	229
$\gamma=10^{-4}$	Winter	19.7	15.9	24.3	13.9	-9.0	65.8	229
$\gamma=10^{-5}$	Winter	19.7	16.0	24.3	13.8	-8.8	65.9	229

Table S3. Comparison between base case simulation results for SO₄²⁻ and observations from CSN network. (Obs. stands for observation; Sim. stands for simulation. Corr. stands for correlation; No. Sites means number of observation site used for statistics.)

Period	Obs. mean	Sim. mean	RMSE	Corr.	MFB	MFE	No. Sites
	$\mu\text{g}/\text{m}^{-3}$	$\mu\text{g}/\text{m}^{-3}$	$\mu\text{g}/\text{m}^{-3}$	%	%	%	
Summer	2.94	3.18	1.75	32.4	12.6	47.2	193
Winter	1.91	1.52	1.06	54.1	-14.9	47.5	193

2 Additional figures

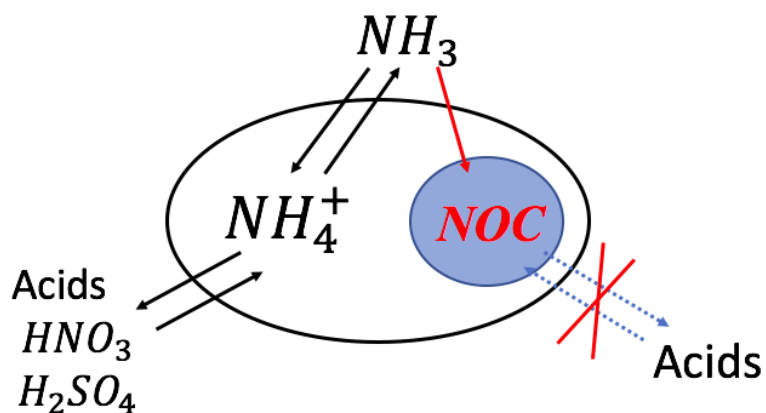


Figure S1. Mechanisms of interactions between NH_3 and particles included in the model: 1) CMAQ already includes reactions between NH_3 and HNO_3 / H_2SO_4 leading to inorganic salts. 2) we are adding a process that converts some (up to 10%) of SOA compounds into NOC which is not basic enough to neutralize acids.

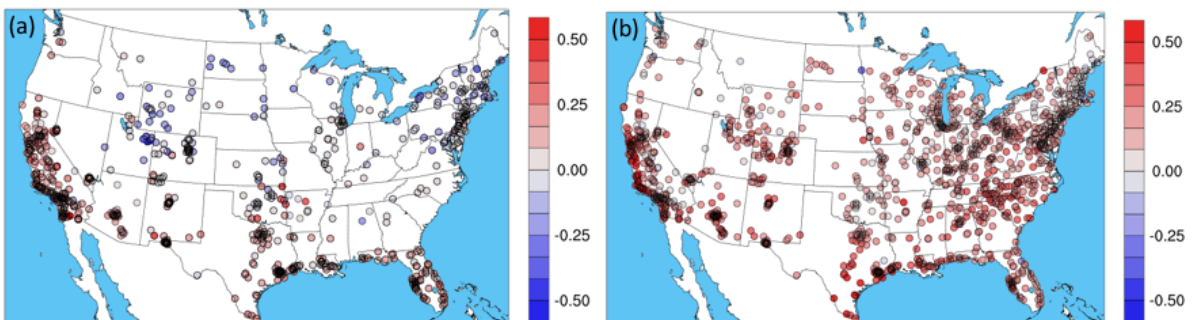


Figure S2. O_3 Mean Normalized Gross Bias at AQS sites for the base case CMAQ model simulation, (a) for winter period, (b) for summer period. Red values indicate an overestimation and blue values indicate an underestimation.

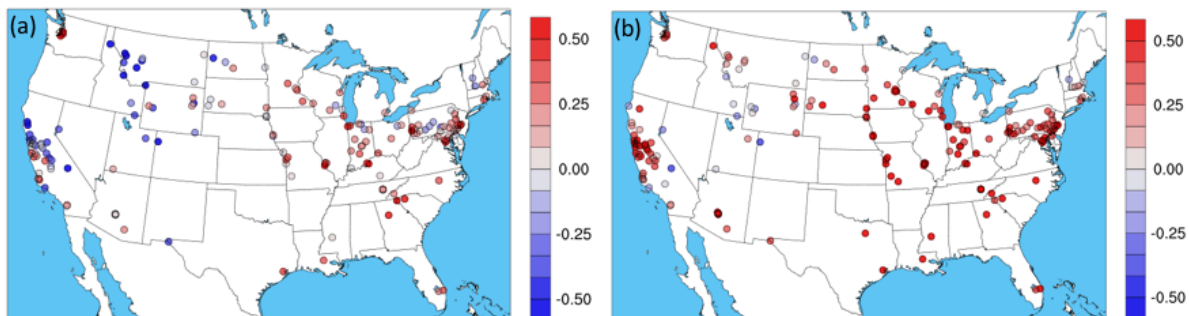


Figure S3. $PM_{2.5}$ Mean Fractional Bias at AQS sites for the base case CMAQ model simulation, (a) for winter period, (b) for summer period. Red values indicate an overestimation and blue values indicate an underestimation.

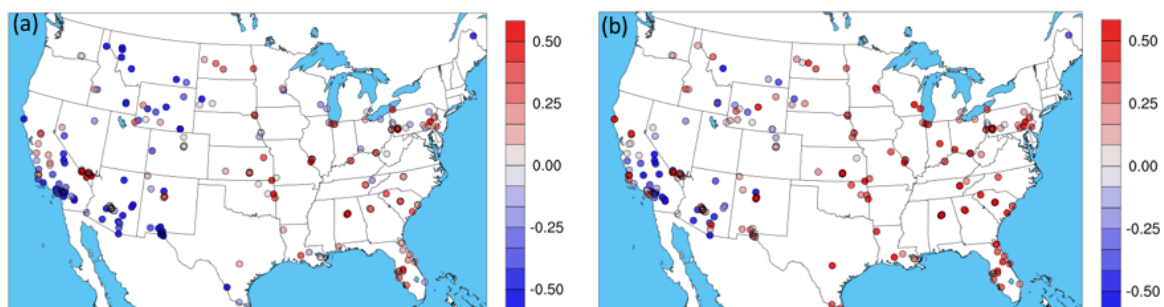


Figure S4. PM_{10} Mean Fractional Bias at AQS sites for the base case CMAQ model simulation, (a) for winter period, (b) for summer period. Red values indicate an overestimation and blue values indicate an underestimation.

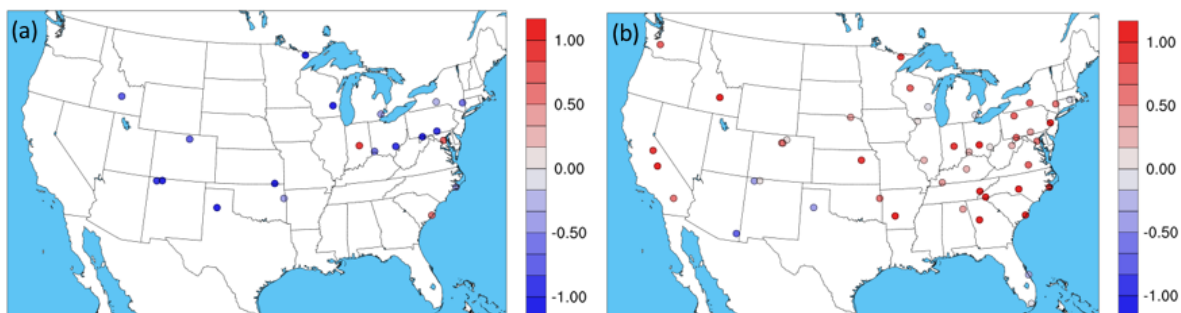


Figure S5. NH_3 Mean Fractional Bias at AMoN sites for the base case CMAQ model simulation, (a) for winter period, (b) for summer period. Red values indicate an overestimation and blue values indicate an underestimation.

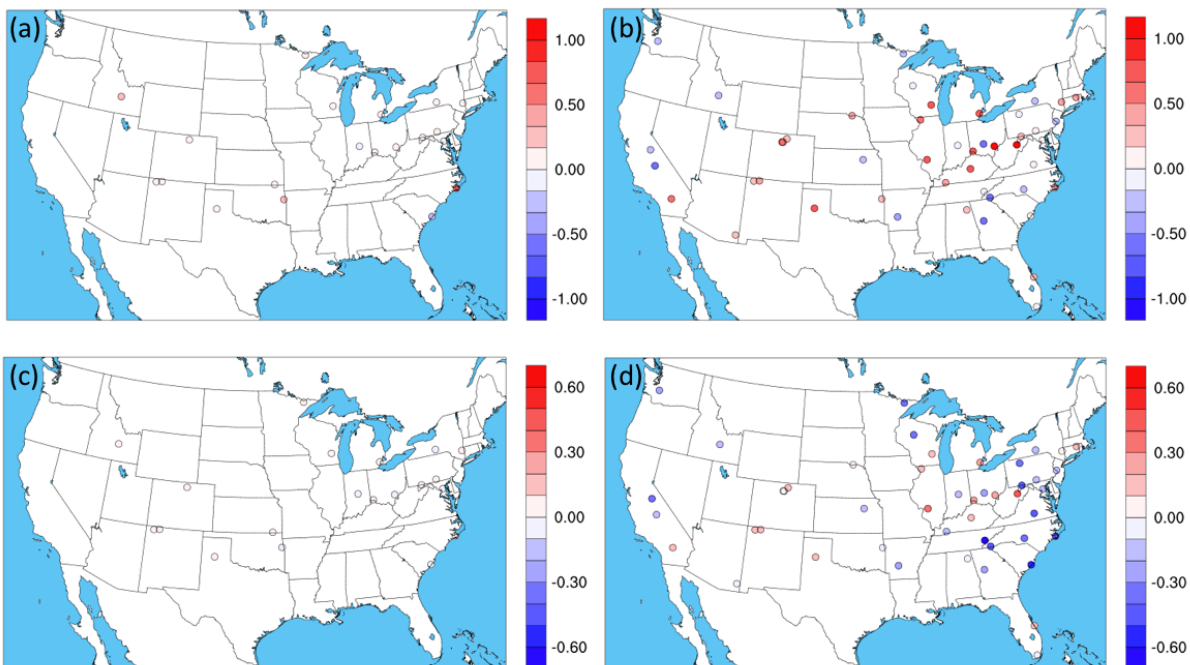


Figure S6. Difference of NH₃ Mean Fractional Error at AMoN sites between the base case, and (a) $\gamma=10^{-3}$ for winter period, (b) $\gamma=10^{-3}$ for summer period, (c) $\gamma=10^{-4}$ for winter period, (d) $\gamma=10^{-4}$ for summer period. Difference for $\gamma=10^{-5}$ are not presented as they are very small. Red values indicate a deterioration of model performance and blue values indicate an improvement of model performance.

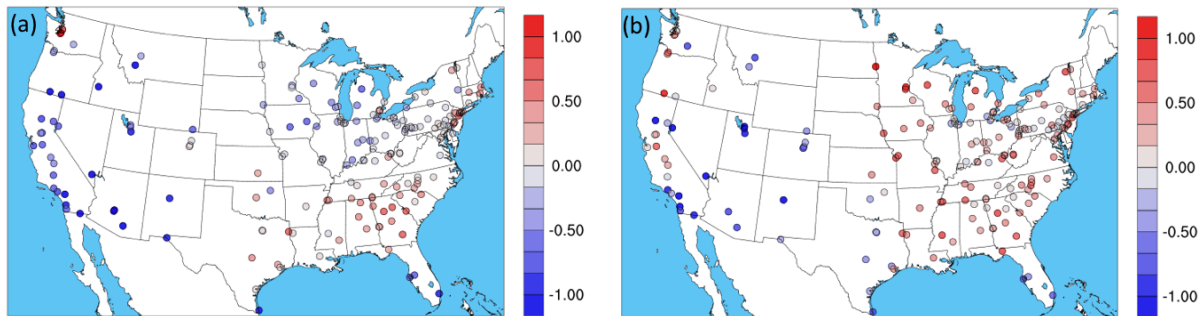


Figure S7. NH₄⁺ Mean Fractional Bias at CSN sites for the base case CMAQ model simulation, (a) for winter period, (b) for summer period. Red values indicate an overestimation and blue values indicate an underestimation.

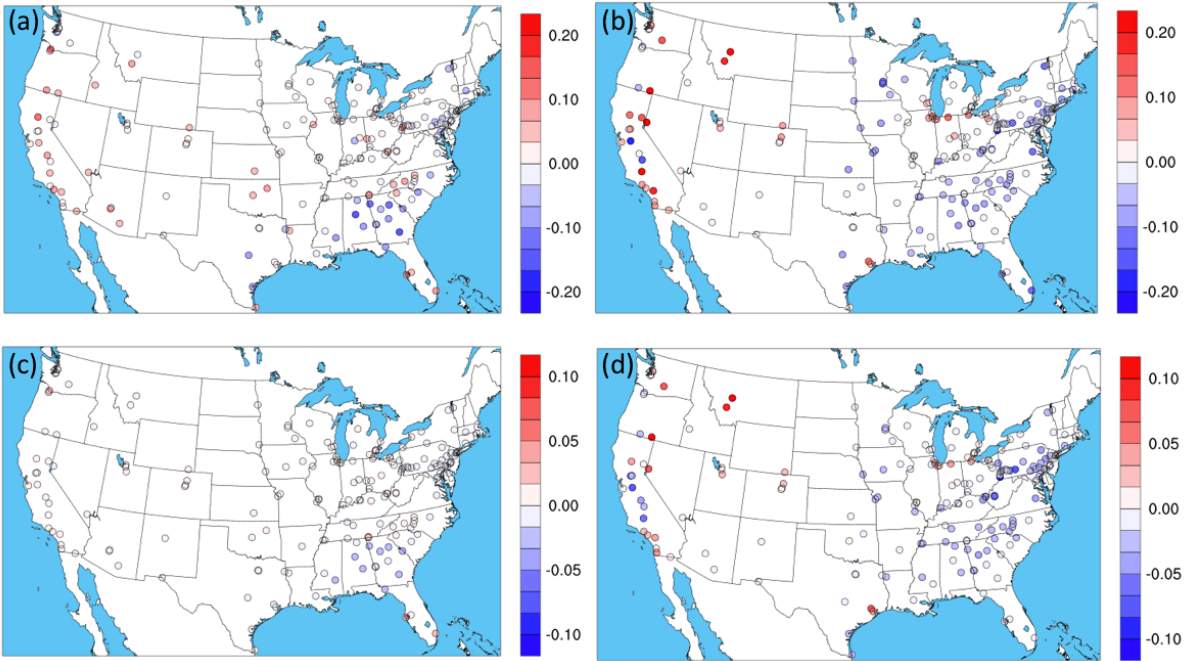


Figure S8. Difference of NH_4^+ Mean Fractional Error at CSN sites between the base case and, (a) $\gamma=10^{-3}$ for winter period, (b) $\gamma=10^{-3}$ for summer period, (c) $\gamma=10^{-4}$ for winter period, (d) $\gamma=10^{-4}$ for summer period. Difference for $\gamma=10^{-5}$ are not presented as they are very small. Red values indicate a deterioration of model performance and blue values indicate an improvement of model performance.

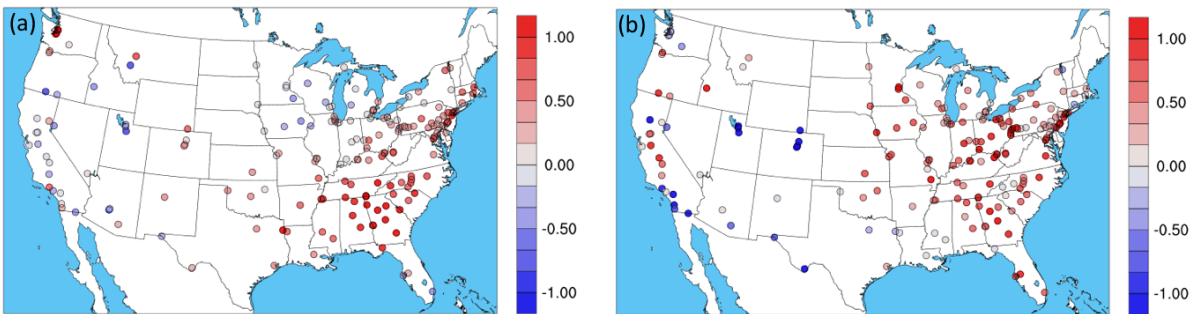


Figure S9. NO_3^- Mean Fractional Bias at CSN sites for the base case CMAQ model simulation, (a) for winter period, (b) for summer period. Red values indicate an overestimation and blue values indicate an underestimation.

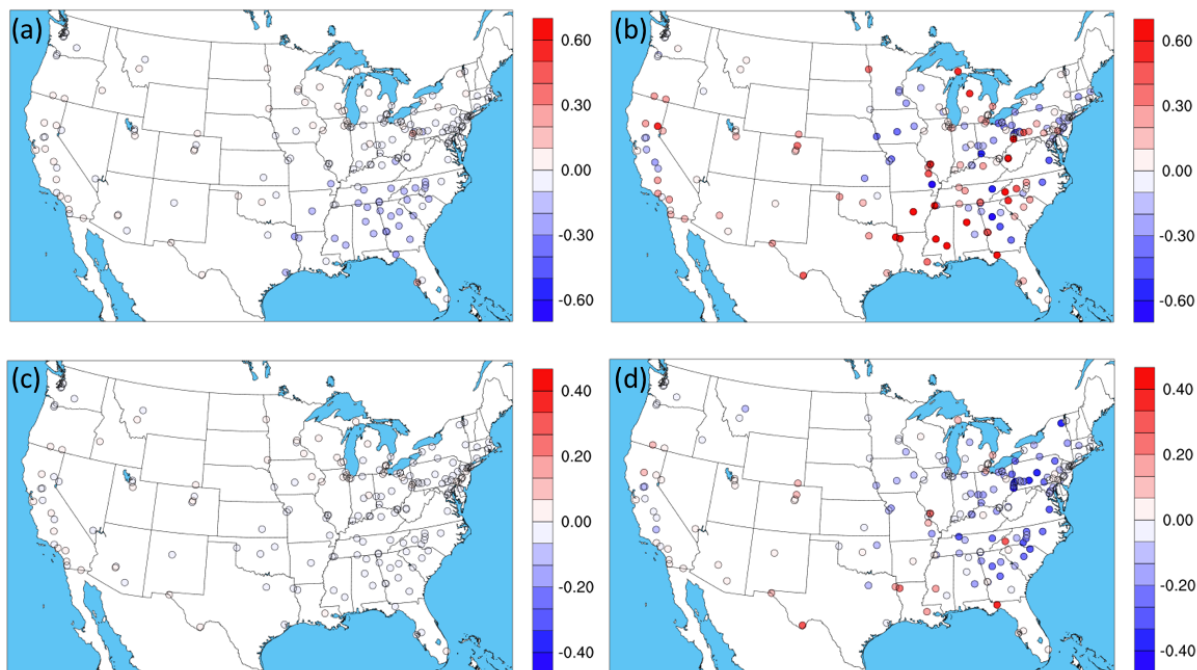


Figure S10. Difference of NO_3^- Mean Fractional Error at CSN sites between the base case and, (a) $\gamma=10^{-3}$ for winter period, (b) $\gamma=10^{-3}$ for summer period, (c) $\gamma=10^{-4}$ for winter period, (d) $\gamma=10^{-4}$ for summer period. Difference for $\gamma=10^{-5}$ are not presented as they are very small. Red values indicate a deterioration of model performance and blue values indicate an improvement of model performance.

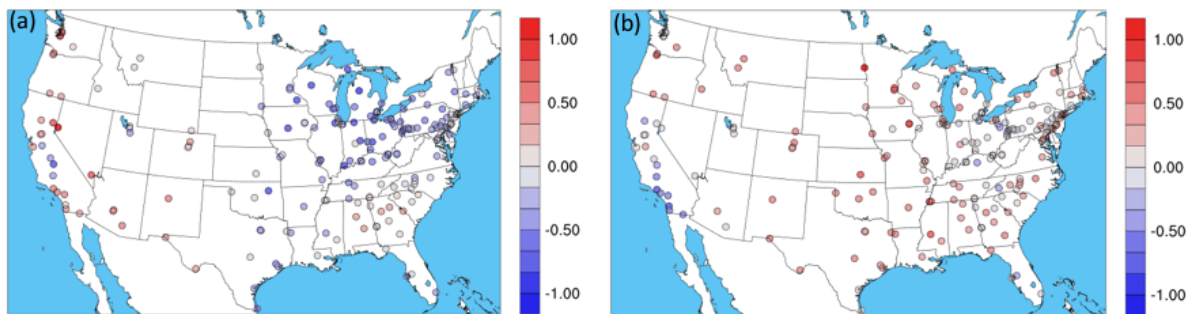


Figure S11. SO_4^{2-} Mean Fractional Bias at CSN sites for the base case CMAQ model simulation, (a) for winter period, (b) for summer period. Red values indicate an overestimation and blue values indicate an underestimation.

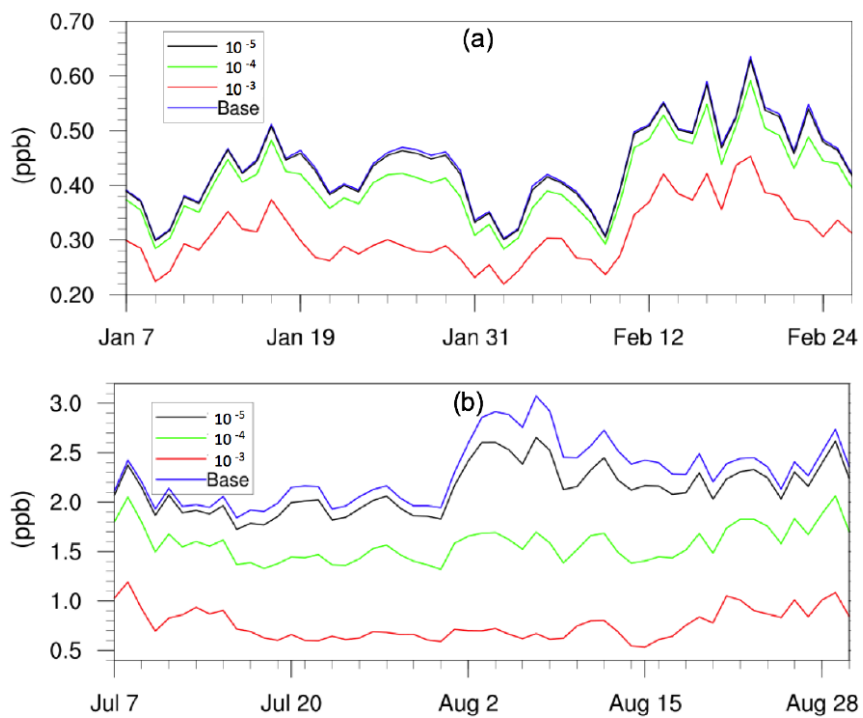


Figure S12. Daily, spatially-averaged NH_3 concentrations for different uptake coefficient scenarios for (a) winter period, and (b) summer period

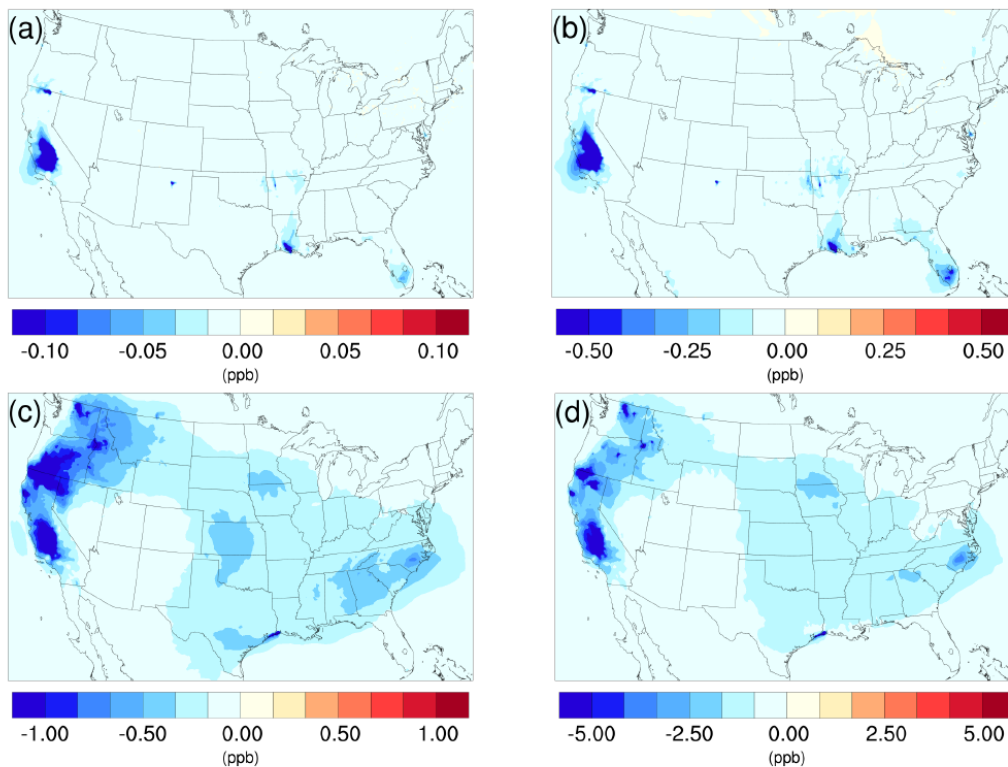


Figure S13. Spatial distribution of the difference in time-averaged NH_3 concentrations between the $\gamma=10^{-5}$ case and the base case for (a) winter period, and (c) summer period and between the $\gamma=10^{-4}$ case and the base case for (b) winter period and (d) summer period.

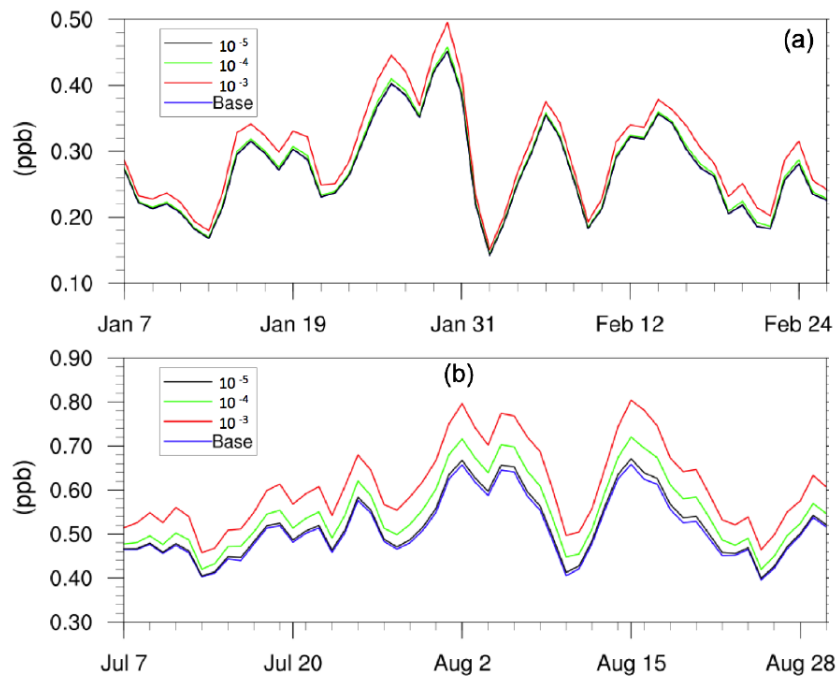


Figure S14. Daily, spatially-averaged HNO₃ concentrations for different scenarios for (a) winter period and (b) summer period

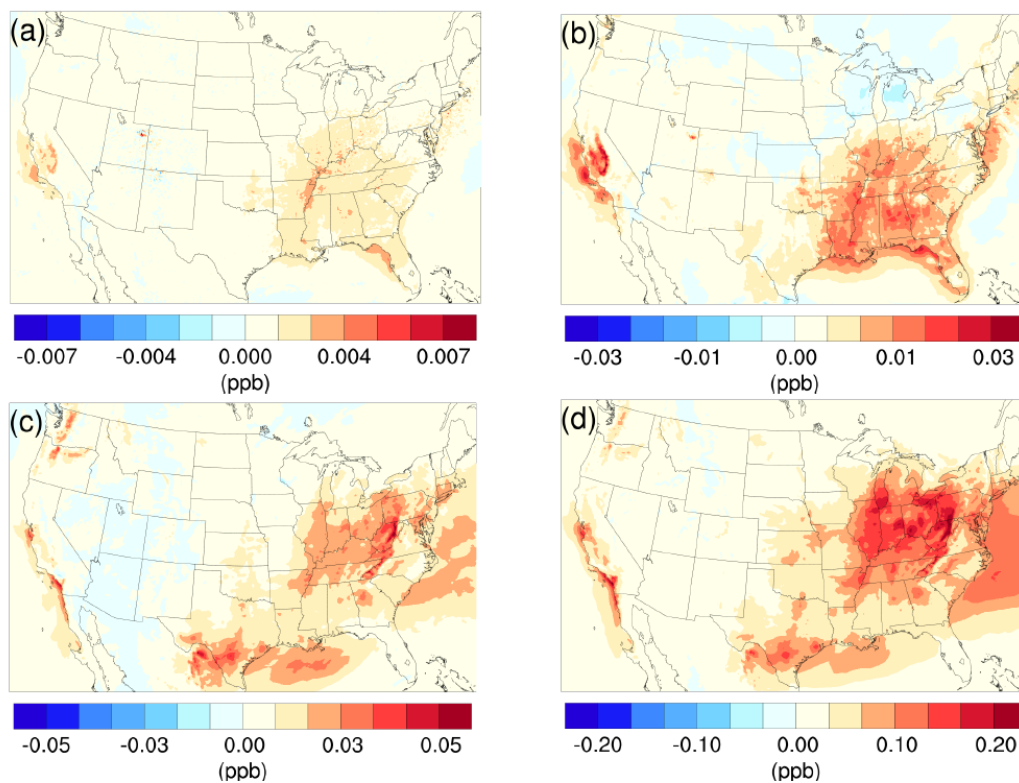


Figure S15. Spatial distribution of the difference in time-averaged HNO₃ concentrations between the $\gamma=10^{-5}$ case and the base case for (a) winter period, and (c) summer period and between the $\gamma=10^{-4}$ case and the base case for (b) winter period and (d) summer period.

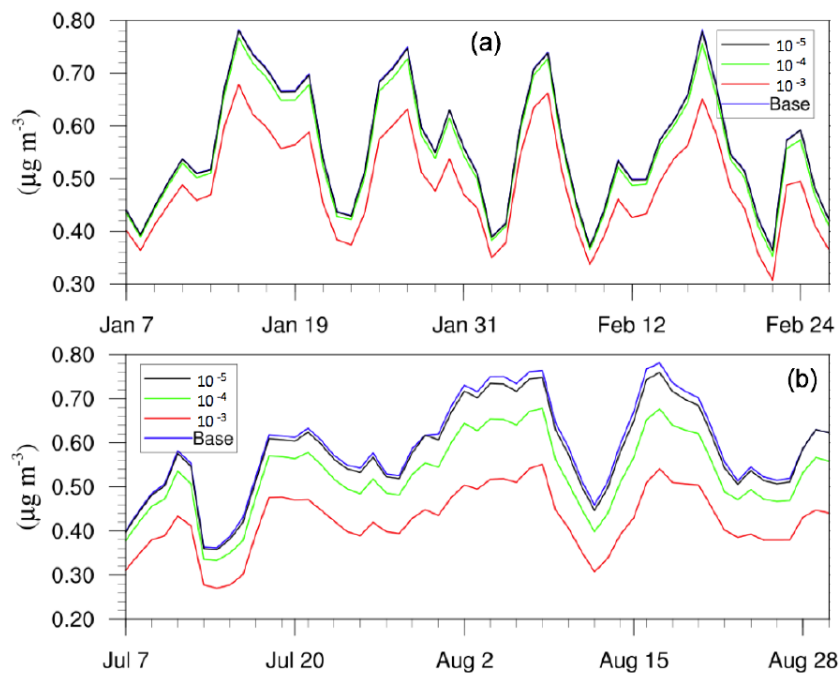


Figure S16. Daily, spatially-averaged NH_4^+ concentrations of different scenarios for (a) winter period, and (b) summer period

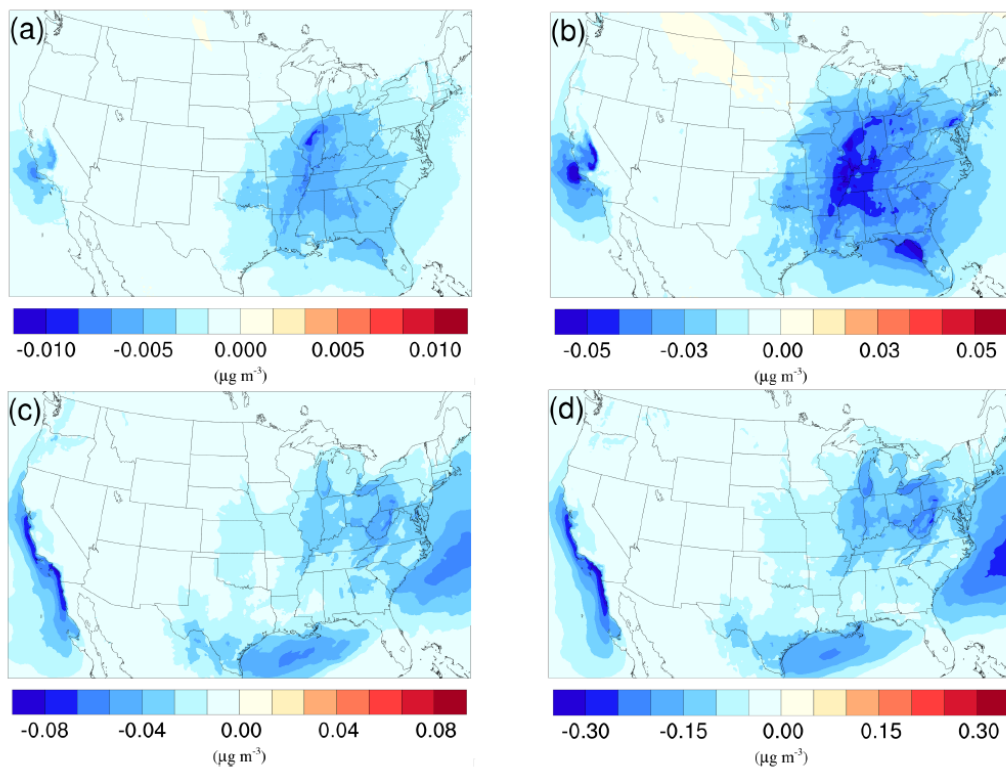


Figure S17. Spatial distribution of the difference in time-averaged NH_4^+ concentrations between the $\gamma=10^{-5}$ case and the base case for (a) winter period and (c) summer period, and between the $\gamma=10^{-4}$ case and the base case for (b) winter period and (d) summer period.

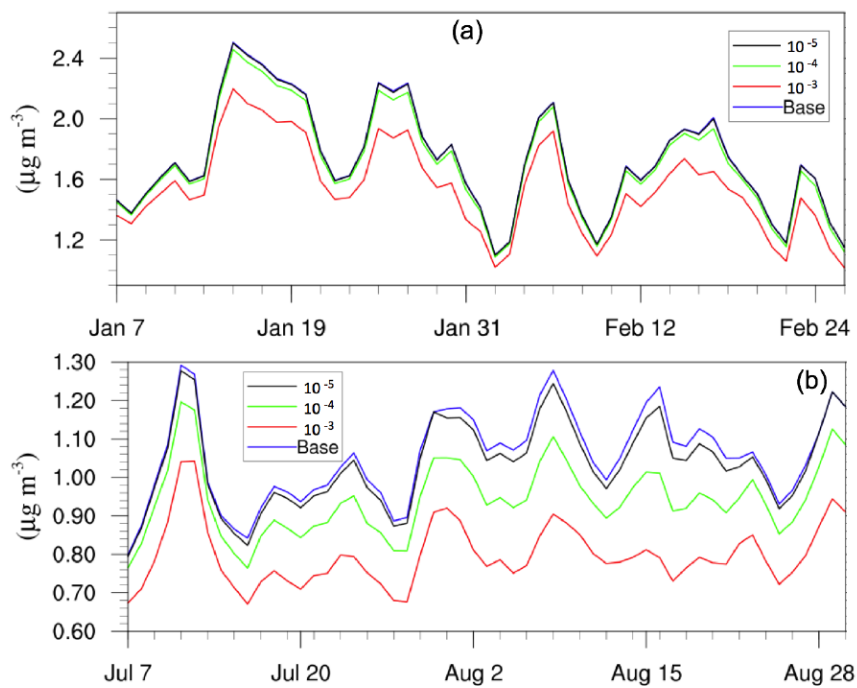


Figure S18. Daily, spatially-averaged NO_3^- concentrations of different scenarios for (a) winter period and (b) summer period

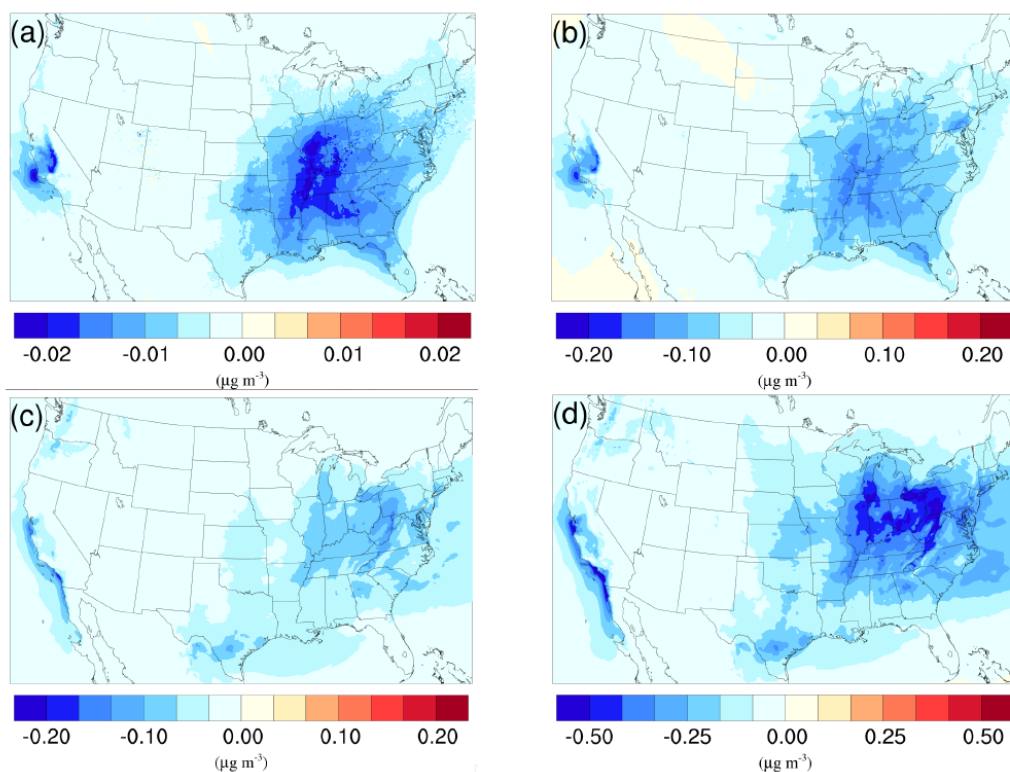


Figure S19. Spatial distribution of the difference in time-averaged NO_3^- concentrations between the $\gamma=10^{-5}$ case and the base case for (a) winter period and (c) summer period and between the $\gamma=10^{-4}$ case and the base case for (b) winter period and (d) summer period.

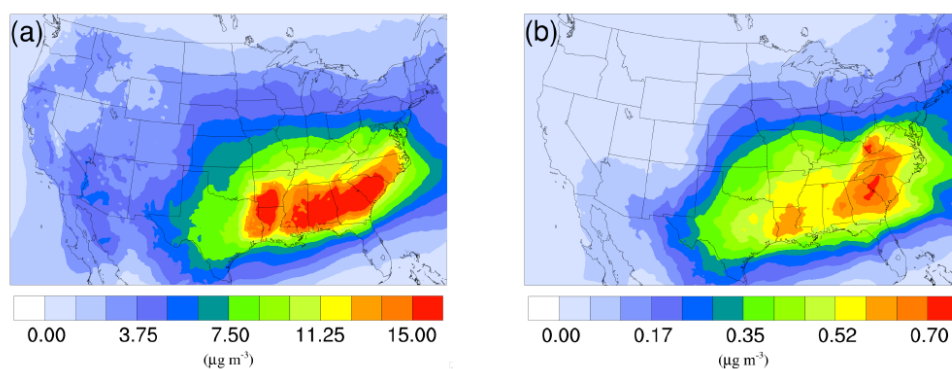


Figure S20. Spatial distribution of time-averaged (a) biogenic SOA concentrations, and (b) the isoprene epoxydiol derived SOA concentrations in the base case for the summer period.

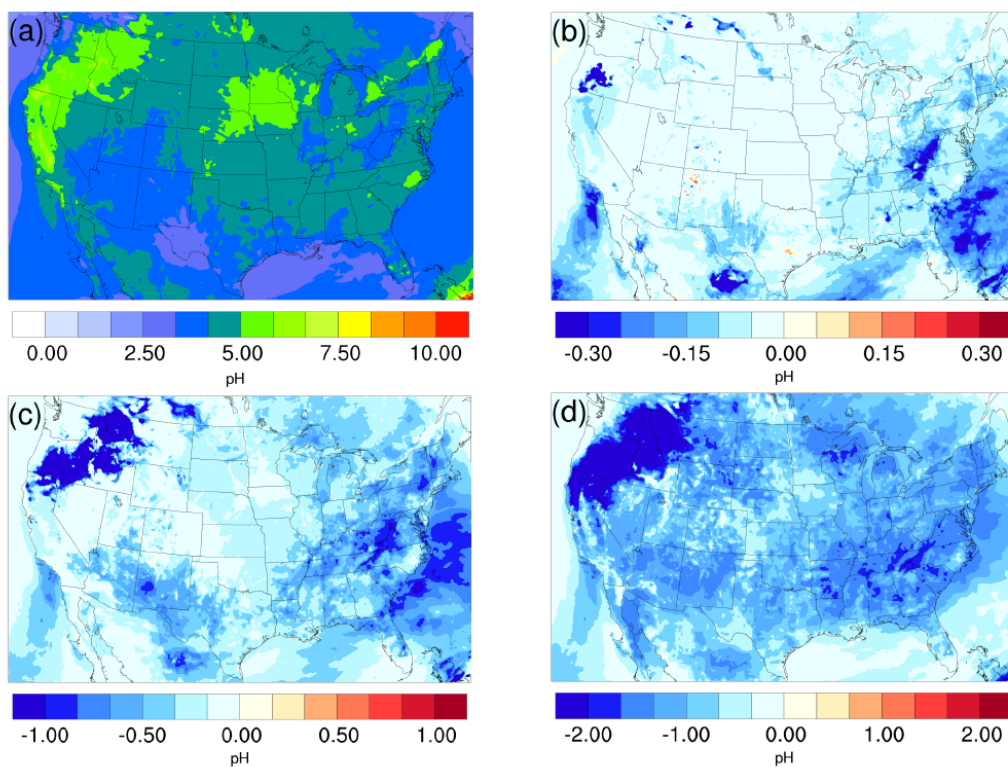


Figure S21. Spatial distribution of time-averaged (a) particle acidity in the base case for the summer period. Spatial distribution of the difference in time-averaged particle acidity between the $\gamma=10^{-5}$ case and the base case, (c) $\gamma=10^{-4}$ case and the base case, (d) $\gamma=10^{-3}$ case and the base case during the summer period.

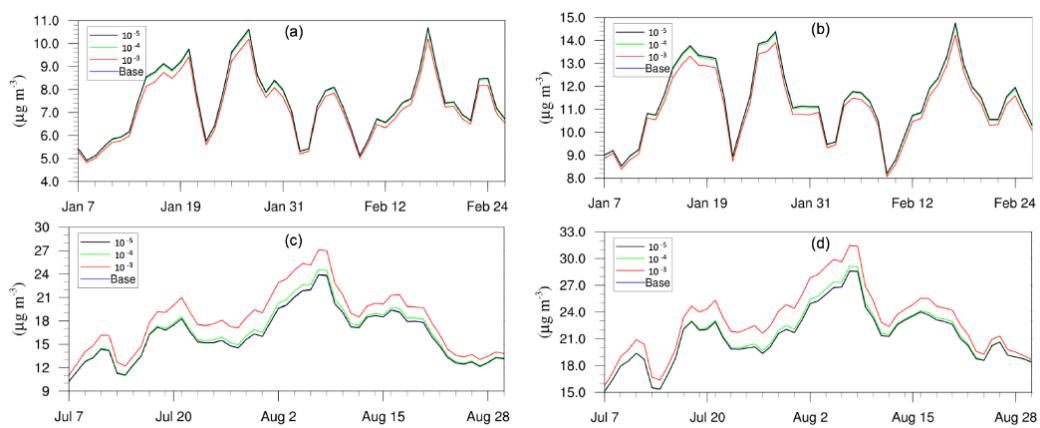


Figure S22. Daily, spatially-averaged concentrations of different scenarios for (a) $\text{PM}_{2.5}$ in winter, (b) PM_{10} in winter, (c) $\text{PM}_{2.5}$ in summer, and (d) PM_{10} in summer

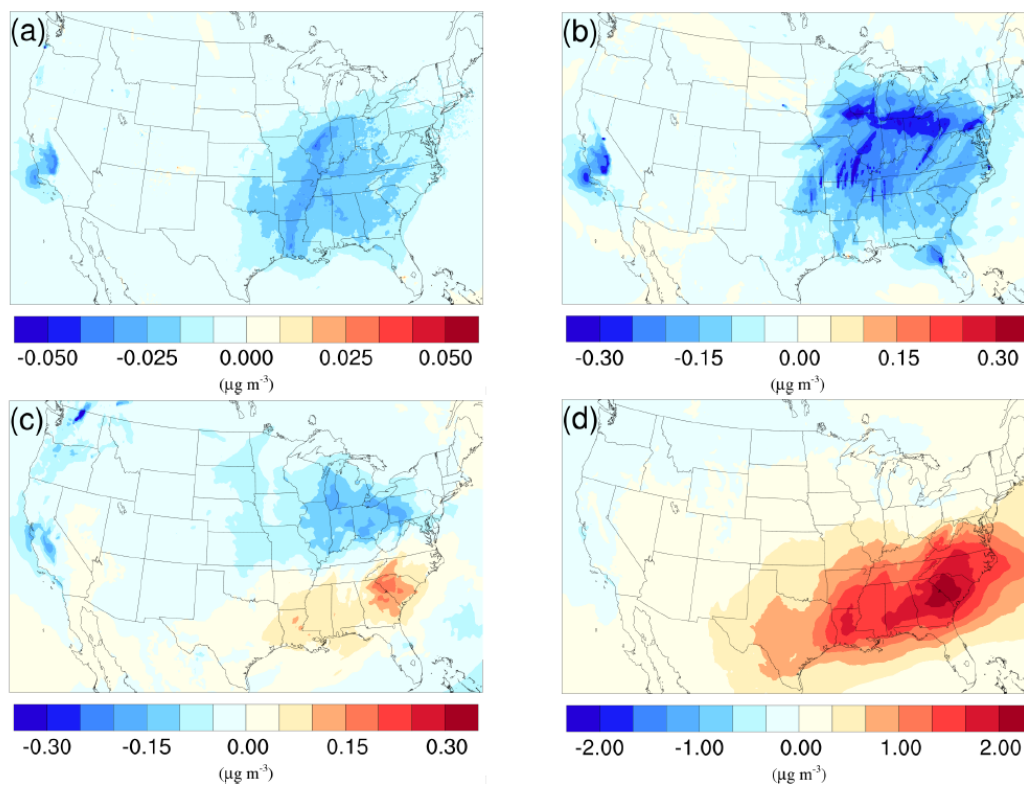


Figure S23. Spatial distribution of the difference in time-averaged PM_{2.5} concentrations between the $\gamma=10^{-5}$ case and the base case for (a) winter period and (c) summer period, and between the $\gamma=10^{-4}$ case and the base case for (b) winter period and (d) summer period.

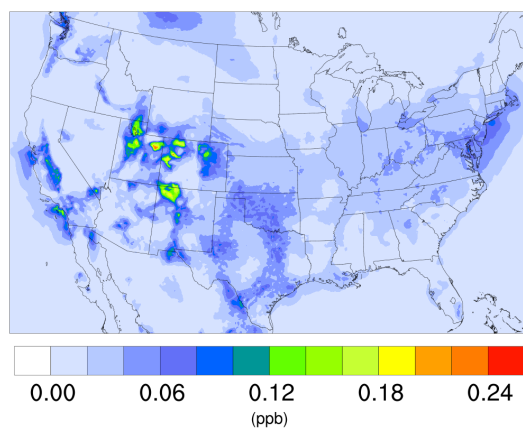


Figure S24. Spatial distribution of averaged N₂O₅ concentration for winter period of the base case.